MEMORANDUM
RM-3228-PR
JULY 1962

SCATTERING AND POLARIZATION PROPERTIES OF POLYDISPERSED SUSPENSIONS WITH PARTIAL ABSORPTION

D. Deirmendjian

PREPARED FOR:

UNITED STATES AIR FORCE PROJECT RAND

The RAND Corporation
SANTA MONICA • CALIFORNIA

MEMORANDUM
RM-3228-PR
JULY 1962

SCATTERING AND POLARIZATION PROPERTIES OF POLYDISPERSED SUSPENSIONS WITH PARTIAL ABSORPTION

D. Deirmendjian

This research is sponsored by the United States Air Force under Project RAND — Contract No. AF 49(638)-700 — monitored by the Directorate of Development Planning, Deputy Chief of Staff, Research and Technology, Hq USAF. Views or conclusions contained in this Memorandum should not be interpreted as representing the official opinion or policy of the United States Air Force. Permission to quote from or reproduce portions of this Memorandum must be obtained from The RAND Corporation.

The RAND Corporation
1700 MAIN ST • SANTA MONICA • CALIFORNIA

PREFACE

The results reported here are derived from a continuing theoretical study of light scattering in atmospheres, supported by the U.S. Air Force under Project RAND. The results have application, not only in the investigation of atmospheres of the earth and other planets, but also in colloid research. This publication has been prepared for presentation at the Interdisciplinary Conference on Electromagnetic Scattering, Potsdam, New York, August 1962, sponsored by The American Chemical Society, and by the U.S. Air Force Cambridge Research Laboratories.

SUMMARY

The angular scattering and polarization properties of polydispersed suspensions of nonabsorbing and partially absorbing spheres have been computed using the complete Mie series. The results with three types of size distributions are presented and compared with observations. These show a strong dependence of angular intensity and polarization patterns on the size distribution, the size range, and the dielectric and absorbing properties of the individual particles. A peculiarity of scattering at angles near 45°, observed experimentally and independently by two authors, is corroborated by the numerical results. Prominent observational features characteristic of natural fog, such as an extremely bright aureole, rainbows and counter coronas are reproduced in a model corresponding to a cloud of spherical water droplets, with a wide distribution in droplet radius and a maximum concentration at a 4-micron radius.

CONTENTS

Scattering and Polarization Properties of Polydispersed Suspensions with Partial Absorption*

Introduction

In studying the theoretical scattering properties of polydispersed suspensions, such as natural hazes and clouds in the atmosphere, two important facts should be considered: (a) Because of the finite size of the particles, even if these are assumed spherical, the angular scattering characteristics cannot be approximated with sufficient accuracy by asymptotic expressions based on geometric optics or Green's function approximations for the internal field. The complete Mie series must be used for each particle. (b) The size distribution function used must reproduce as faithfully as possible the size spectrum of the suspension in question.

In this paper we shall present briefly examples simulating atmospheric water clouds and hazes with size distributions that are sufficiently realistic to allow comparisons with observational data. The capabilities of modern high-speed computers in generating single-particle Mie scattering functions, both with real and complex index of refraction, has been adequately described elsewhere (Deirmendjian, et al, 1961; Giese, 1961). Therefore we shall describe only the

---

*Parts of this paper were presented at the International Symposium on Radiation of the Radiation Commission, I.A.M.A.P., Vienna, August 1961.

size-distribution functions used and justify their choice.

Size-distribution function

The function chosen is a generalization of that first proposed by Khrgian and Mazin (1952, 1956) for clouds. A survey of various proposed functions showed that the latter type seems to fit fairly well with measurements both on natural water clouds and aerosols, and it has the great advantage that its parameters have readily interpretable physical meaning. In its most general form this function may be written

$$n(r) = a\, r^{\alpha}\, e^{-br^{\gamma}} \tag{1}$$

where $n(r)$ is the volume concentration at the radius r and $\underline{a}$, $\underline{\alpha}$, $\underline{b}$ and $\underline{\gamma}$ are positive constants. For a particular choice of α and γ, the remaining constants can be uniquely determined by the total number of particles N per unit volume, and by the critical or mode radius r_c, where the concentration is at a maximum. Thus the constant $\underline{a}$ can be determined from the integral

$$N = \int_0^{\infty} n(r)dr = \frac{a}{\gamma}\, b^{-\frac{\alpha+1}{\gamma}}\, \Gamma\left(\frac{\alpha+1}{\gamma}\right), \tag{2}$$

and $\underline{b}$ from the derivative, which can be written

$$\frac{d}{dr}\, n(r) = a\, r^{\alpha-1}\, e^{-br^{\gamma}}\, (\alpha - \gamma b r^{\gamma}) \tag{3}$$

which vanishes when

$$b = \frac{\alpha}{\gamma r^{\gamma}} \quad , \quad r = r_c \tag{4}$$

as well as for $r = 0$ and ∞.

In particular, with the choice $\alpha = 6$, $\gamma = 1$, $r_c = 4\mu$, and $N = 100\ cm^{-3}$ as a nominal concentration, one gets the distribution function

$$n(r) = 2.373\ r^6\ e^{-1.5r}\ cm^{-3}\ \mu^{-1} \tag{5}$$

when the radius is expressed in microns and the concentration per cubic centimeter. This model, marked "cloud" in Fig. 1, reproduces fairly well some of the distributions found by Durbin (1959) for cumulous clouds having a depth between 230 and 2100 m, as averaged and reproduced as "cumulus Type I" in a diagram by Singleton and Smith (1960).

The discontinuous distribution called "haze C" in Fig. 1 roughly approximates the continental hazes measured by various workers and used by the author previously (Deirmendjian 1957, 1959, 1960).

The other continuous distribution in Fig. 1, marked "haze M" is obtained by putting $\alpha = 1$, $\gamma = 1/2$ in (1) with $r_c = 0.05\mu$, resulting in the specific function

$$n(r) = 5.33 \times 10^4\ re^{-8.944\sqrt{r}} \tag{6}$$

This was found to agree with unpublished counts of aerosol particles made in Los Angeles by J. Y. Gilbert (1954), and may be taken to represent coastal conditions. The differences from the model C haze are considerable, in that there is a much larger concentration of

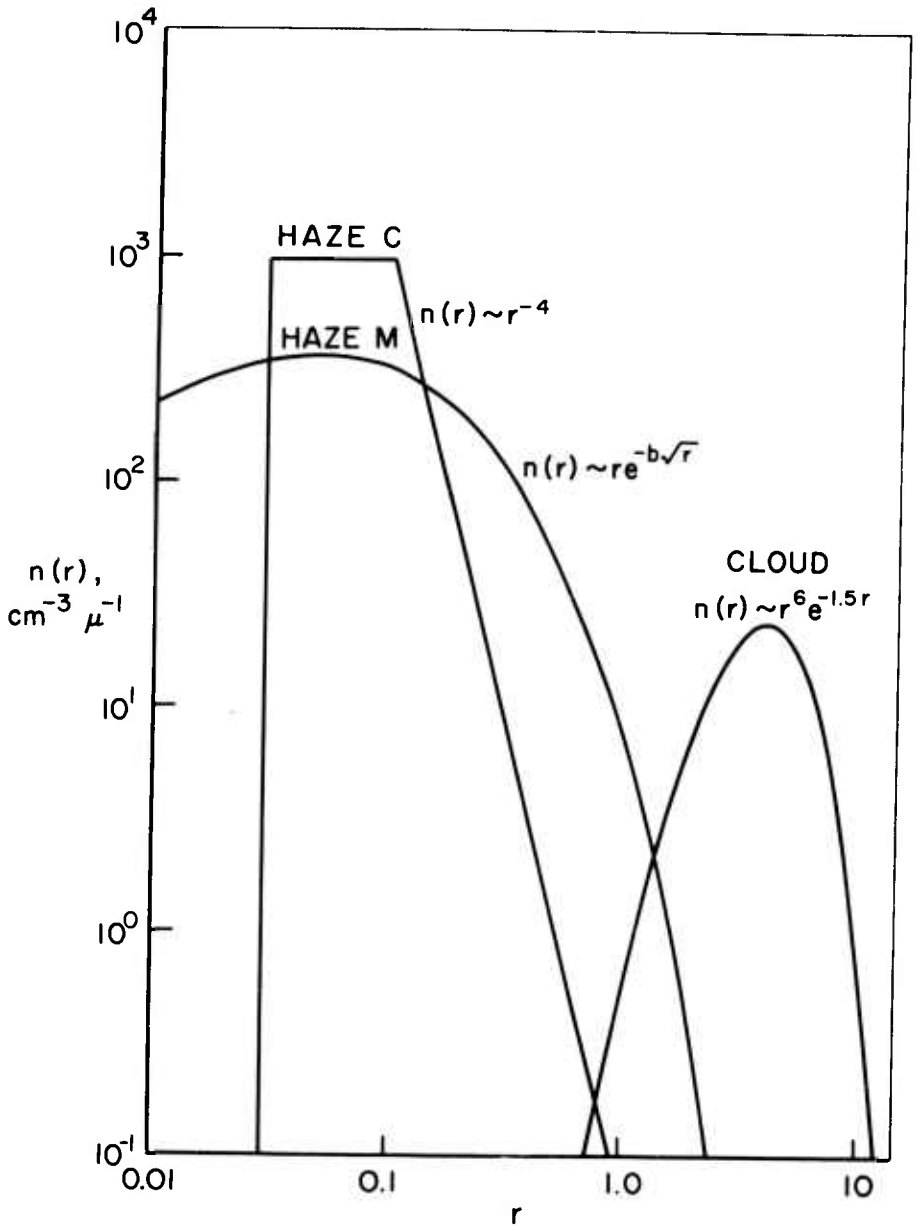

Fig.1— Three size-distribution functions used in the integration of the Mie functions. Total concentration 100 cm^{-3}

particles in the 0.15-to 3.5-micron range. The distribution (6) seems also to correspond fairly well to that of stratospheric aerosols found by Junge, Chagnon and Manson (1961), at least in the range $0.2 < r < 1\mu$.

The logarithmic representation in Fig. 1 is chosen for convenience only and does not give a good idea of the distribution. A linear representation of the continuous distributions would result in bell-shaped curves which are skewed toward the larger sizes. However, since the integrals under all three distributions in Fig. 1 give 100 particles per cubic cm, the curves do provide an idea of the relative amounts in each size interval.

Integration of the Mie functions with size distribution

To get the total scattering and absorption cross-sections per unit volume of the cloud or haze, one has to integrate the Mie single-particle cross-sections with respect to the appropriate distribution. Making the convenient change of variable $r = k^{-1}x$, where x is the Mie size parameter and $k = 2\pi/\lambda$ is the free-space propagation constant at the wavelength λ, one can rewrite the size distribution function (1) in the form

$$f(x,k) = a\, k^{-3-\alpha}\, x^{\alpha} \exp\left\{ - b\, (x/k)^{\gamma} \right\} \qquad (7)$$

where the factor k^{-3} is introduced for convenience. It is easy to show then that the volume cross-sections β may be obtained by the integration

$$\beta(m,\lambda;\, x_1,x_2) = \pi \int_{x_1}^{x_2} x^2\, f(x,k)\, K(m,x)\, dx \qquad (8)$$

where m is the complex or the real index of refraction of the particles, K is the Mie extinction, scattering, or absorption cross-section, as the case may be, divided by the geometrical cross-section (Deirmendjian et al., 1961), and x_1 and x_2 correspond to the lower and upper limits in the particle size.

The elements of the normalized scattering matrix or phase matrix as defined by Chandrasekhar (1950), are given by the integrals

$$\frac{P_j}{4\pi}(m,\theta,\lambda;x_1,x_2) = \frac{1}{\beta_{sc}}\int_{x_1}^{x_2} f(x,k)\, i_j(m,x,\theta)dx,\ j = 1,2,3,4 \quad (9)$$

where θ is the scattering angle, and $i_j(m,x,\theta)$ are the dimensionless Mie intensity functions computed previously (Deirmendjian, 1961), related to the intensity or phase matrix operating on the Stokes vector of the incident radiation in the manner indicated by various authors (Sekera, 1957; van de Hulst, 1957).

It is in the behavior of the integrals (8) and (9) as a function of x_2 that the advantage of the distribution functions of the type (1) becomes evident. Numerical tests using our IBM7090 program show, in fact, that in this case, these integrals always converge to a constant value for all $x_2 > X$, where X is a finite number depending on the logarithmic derivative of the function n(r) with respect to r. In particular, it appears that a sufficient condition for convergence to begin, for all integrals (8), (9) <u>including the forward scattering</u> case with $\theta = 0$, is that r_2 (or correspondingly x_2) be such that

$$-\frac{d}{d \log r}\log n(r) = \alpha\left[\left(\frac{r}{r_c}\right)^{\gamma} - 1\right] > 4 \quad (10)$$

Solving the inequality to the right, we get the condition for convergence to begin

$$r_2 > r_c \, (1 + 4/\alpha)^{1/\gamma} \qquad (11)$$

This is a very convenient property in regard to the contribution of the larger particles in a suspension, where the corresponding Mie series are very long and machine computation time becomes costly. It is also a physically justifiable feature of long-lived atmospheric aerosol and cloud particles, which are naturally limited in the maximum size. Distributions such as model C with $n(r) \sim r^{-4}$ are not convenient because the integrated volume extinction, and scattering in the forward area depend on the choice of the upper limit r_2.

The numerical results further show that, for x_2 in the region defined by (11), the integrals (8) and (9), when plotted as a function of x_2, are smooth and monotonic curves, with little change in value when the integration interval Δx is varied. This is a remarkable property, connected with the choice of <u>continuous</u> size distribution functions of the type (1), since it is known (Penndorf, 1962; Deirmendjian, et al, 1961), that the intensity for single particles, especially in the backward hemisphere, shows large fluctuations as a function of the size, whose amplitude and frequency increase with x. It means that the angular scattering pattern of polydispersed suspensions, with a more or less wide and continuous size spectrum, should be a smooth function of θ, without the numerous coronas, rainbows and countercoronas characteristic of single particles or monodispersed suspensions.

It should be noted from the form of the integral (9) that the phase functions are independent of the total concentration N of particles per unit volume, as should be evident from physical considerations. This statement is of course valid only when the concentration is small enough that only incoherent or independent scattering need be considered.

Volume extinction and albedo

Examples of the extinction per unit path for the three models and at selected wavelengths are shown in Table 1. The particles are assumed to be made of liquid water, with the real or the complex index of refraction indicated in Table 1, adapted from Centeno (1941). The table also lists the computed albedo A per unit volume of space, that is, the fraction of energy scattered in all directions weighted by the distribution function, compared to that scattered and absorbed. The numbers in Table 1 illustrate clearly the effects of changes in distribution function, in the relative size, and in the index of refraction of the particles. Noted particularly are the similarities and differences between the two haze models. The lower albedo for model C at $\lambda 3.07\mu$ and $\lambda 6.05\mu$ is explained by the larger proportion of small particles in it as compared to model M (see Fig. 1), such particles being relatively more efficient real absorbers than the larger ones for any given complex index. These differences are even more pronounced when comparing the haze and cloud distributions, especially at $\lambda 10\mu$.

The extinction values for the cloud model show the interesting fact that these should increase with wavelength in the near-infrared

Table I

Volume Extinction Coefficient and Albedo

			Haze C (2300 cm^{-3}, $r_2 = 5\mu$)		Haze M (100 cm^{-3}, $r_c = 0.05\mu$)		Cloud (100 cm^{-3}, $r_c = 4.0\mu$)	
λ	Re $\{m\}$	Im $\{m\}$	β_{ext} km^{-1}	Albedo A (β_{sc}/β_{ext})	β_{ext} km^{-1}	Albedo A	β_{ext} km^{-1}	Albedo A
0.45μ	1.34	0	0.1206	1.0	0.1056	1.0	16.33	1.0
1.61μ	1.315	0	0.0312	1.0	0.0691	1.0	17.58	1.0
3.07μ	1.525	0.0682	0.0289	0.620	0.0602	0.721	18.58	0.529
3.90μ	1.353	0.0059	0.0128	0.930	0.0236	0.948	20.65	0.914
5.30μ	1.315	0.0143	0.0075	0.800	0.0112	0.826	24.01	0.884
6.05μ	1.315	0.1370	0.0129	0.260	0.0189	0.297	19.86	0.543
10.0μ	1.212	0.0601	0.0032	0.202	0.0045	0.178	11.18	0.601
16.6μ	1.44	0.4000	0.0082	0.104	0.0134	0.075	16.97	0.395

region, even though the relative size decreases, partly because of the increase in the absorption coefficient of liquid water.

A comparison of the corresponding extinction coefficients under Table 1 for the model C haze, with those approximated previously by Deirmendjian (1960) by means of an empirical extension of van de Hulst's (1957) analytical approximation, shows very good agreement, indicating the sound basis of van de Hulst's original analysis. Those corresponding to a cloud also agree in order of magnitude and wavelength dependence, but not in detail, because a different model, with $r_c = 3.5\mu$ and a narrower symmetrical distribution, was used in the earlier approximate calculation by Deirmendjian (1960).

Normalized intensity functions P_1 and P_2

Figures 2 to 9 represent examples of the integrated intensity functions of phase matrix elements $P_1/4\pi$ (solid line) and $P_2/4\pi$ (dashed lines) which are normalized so that they satisfy the condition:

$$\frac{1}{8\pi}\int_{\Omega}\left[P_1(\theta) + P_2(\theta)\right]\, d\omega = 1 \qquad (12)$$

The ordinates in all these figures are on a logarithmic scale, while the abscissa is linear in the scattering angle θ measured from the forward direction. For unpolarized and parallel monochromatic incident energy of unit flux, the degree of partial linear polarization is given by the ratio

$$\frac{P_1(\theta) - P_2(\theta)}{P_1(\theta) + P_2(\theta)}$$

with positive values corresponding to maximum electric-vector amplitude perpendicular to the scattering plane. The maximum numerical value and position of this parameter is indicated on all eight figures.

Figure 2 corresponds to a model C water haze (maximum particle radius of 5μ) illuminated by infared radiation at $\lambda 5.3\mu$. The scattering pattern is smooth with strong anisotropy equivalent to a ratio of 10^2 between forward and backward scattering. A maximum positive polarization of 0.71 occurs at $\theta = 100^\circ$, explained by the small relative size of the particles and their absorption properties.

Figure 3 shows the scattering pattern for the same haze when illuminated by visible light at $\lambda 0.45\mu$, where the refractive index of water is assumed real and equal to 1.34. If Fig. 3 is compared to Fig. 2, it is seen that the anisotropy has increased by one order of magnitude and the maximum polarization, though still at $\theta = 100^\circ$, has decreased in value to 0.49. Both changes are due to the larger relative size of the particles. The pattern for $\lambda 0.70\mu$ radiation (not shown) is similar except that the maximum at $\theta = 0$ is reduced by about 62 per cent.

Figures 4 and 5 correspond to the situation for a water haze with a distribution according to model M, at the wavelengths of 0.70 and 0.45μ respectively. The intense aureole in the region $0^\circ < \theta < 10^\circ$, is more pronounced at the shorter wavelength here than in model C, with a reduction of 50 per cent at $\lambda 0.70\mu$. Another difference is in the polarization pattern, which has migrated toward larger angles with a maximum of about 0.40 at $\theta = 152^\circ$. In the region $20^\circ < \theta < 100^\circ$, the polarization is weak and negative. All

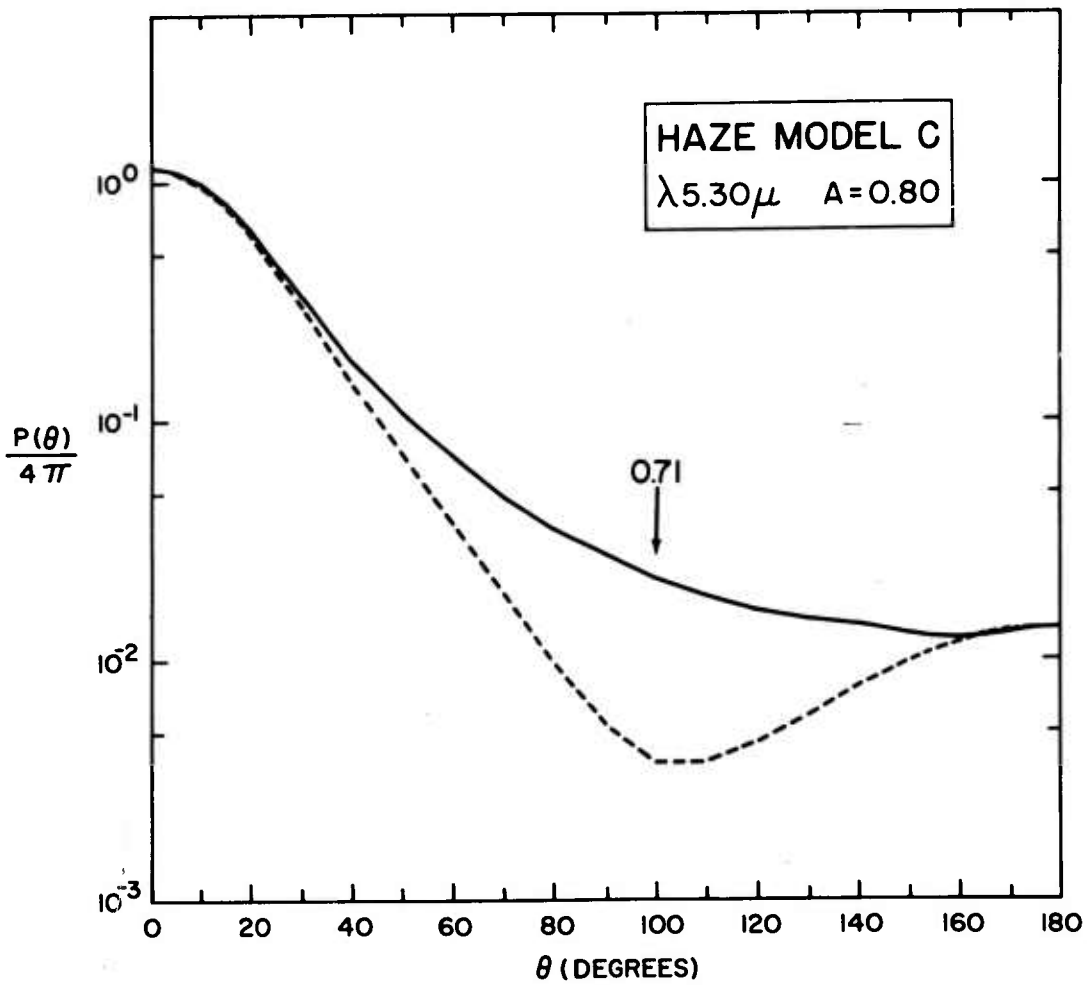

Fig. 2

Integrated and normalized intensity functions $P_1/4\pi$ (solid line) and $P_2/4\pi$ (dashed line) for haze particles with complex index (see Table 1) and infrared illumination. Computed values at θ: 0(5)20(10)150(5)180° joined by straight lines.

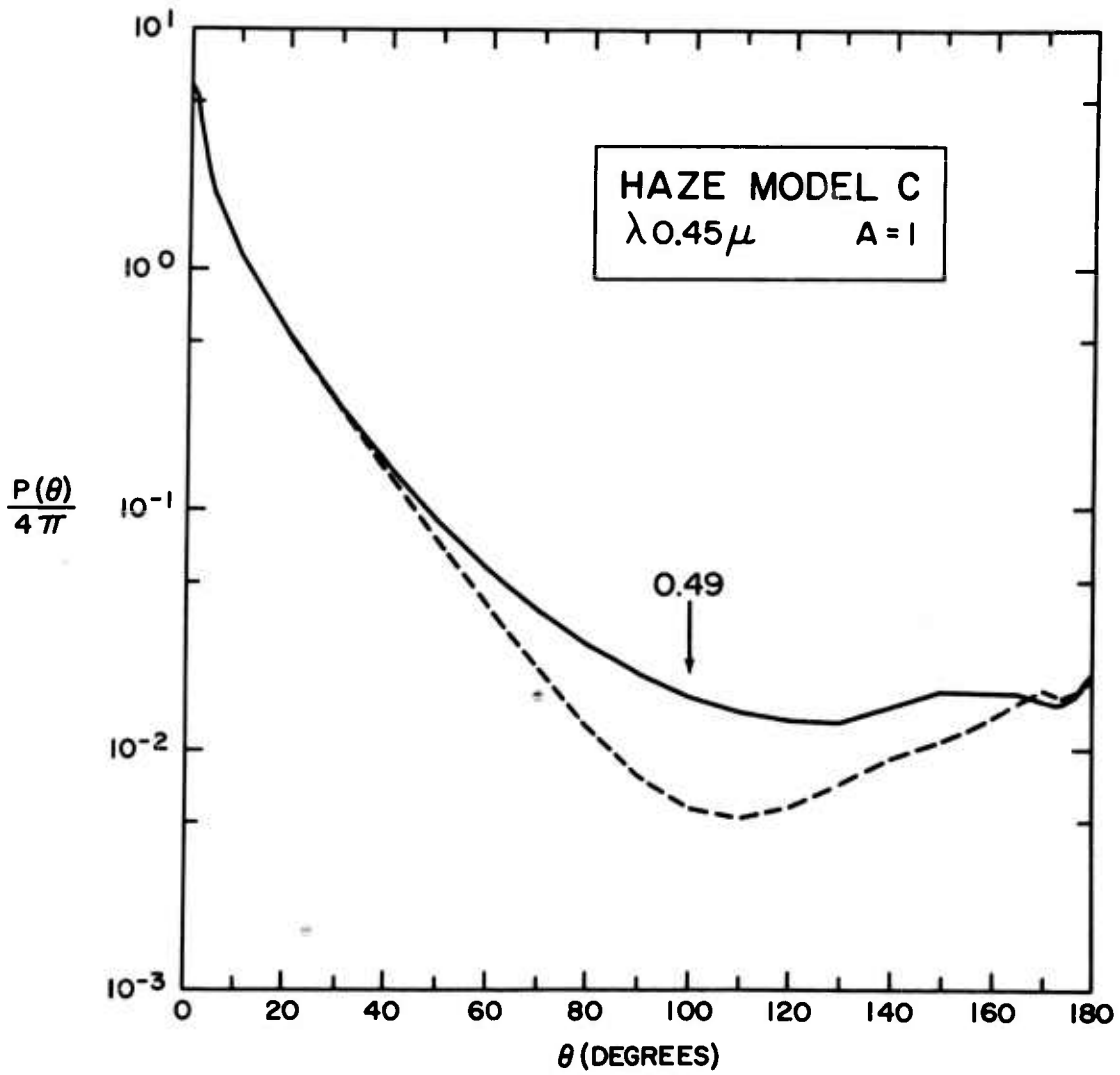

Fig. 3

Same as Fig. 2 but for particles with real index and visible light. Computed values at θ: 0(1)5,10(10)150(5)170(2)180°.

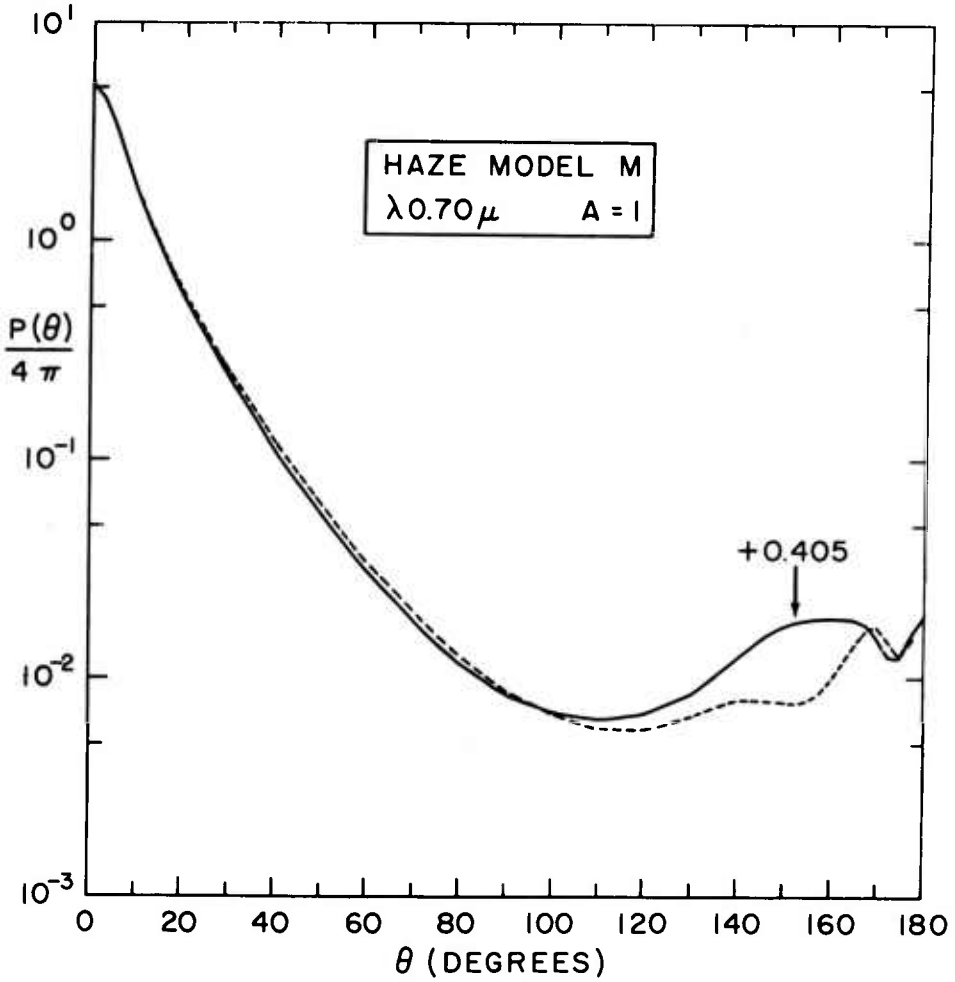

Fig.4—Intensity functions for haze particles at λ0.70μ and with real index 1.33 but a different distribution than in Fig. 3
Computed values at θ: 0(2.5) 20(10) 130(2.5) 180°

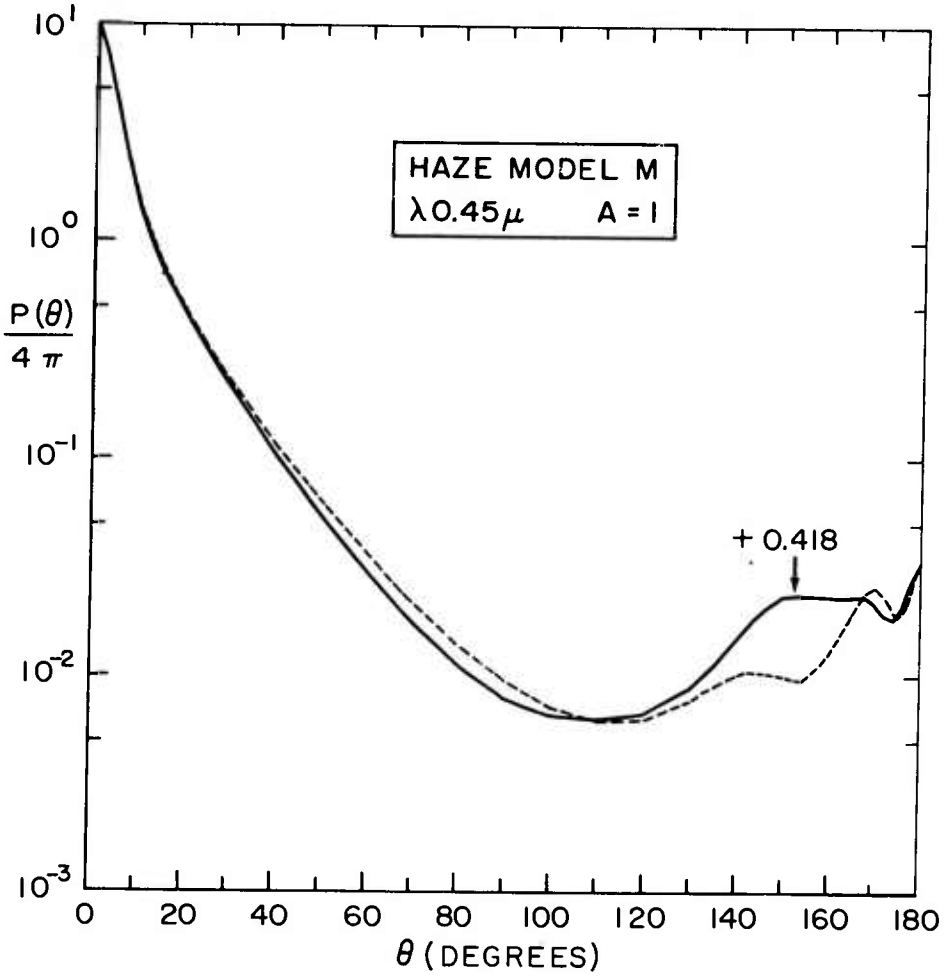

Fig.5 — Same as Fig.4 but with illumination at λ0.45μ, with real index 1.34

these changes in going from a model C to a model M distribution are connected with the relatively larger amount of particles in the range $0.15<r<3.5\mu$ in the second model as compared to the first (see Fig. 1).

In general, the unit-volume scattering characteristics by the haze particles must be closely related to the deviations of the observed degree of polarization and the position of the neutral points in the sunlit sky from those predicted by Rayleigh multiple scattering, as discussed by Sekera (1957) and others. More particularly, it can be shown (Deirmendjian, 1959) that the most prominent deviations should appear in the brightness of the region around the sun called the aureole, which can be easily explained by the effect of primary scattering of sunlight on haze particles. In fact, the normalized intensity function $P_A(\theta)$ for a mixture of air and particles may be written in the form

$$P_A(\theta) = \frac{\beta_R P_R(\theta) + \beta_M P_M(\theta)}{\beta_R + \beta_M} \qquad (13)$$

where the subscripts R and M stand for Rayleigh and Mie particles respectively. Usually, even on clear days, the attenuation coefficients β_R and β_M in the visible range, are of the same order of magnitude, whereas for small scattering angles say $\theta<5^\circ$, $P_M \simeq 100\ P_R$, where $P_M \equiv \frac{1}{2}(P_1+P_2)$ and $P_R = \frac{3}{4}(1+\cos^2\theta)$. Thus, at such angles, the large particle effect will dominate in the brightness (and hence also in the polarization).

In this connection, it is important to introduce the correct gradient and intensity of the aureole in estimates of the volume

scattering coefficient based on an integration of the angular intensity over all solid angles. Extrapolations of the angular intensity in the region $0^\circ \leqq \theta < 10^\circ$, when the corresponding data are unavailable, may lead to an incorrect estimate of both the volume scattering coefficient and the anisotropy between forward and back scattering, and hence also of the wavelength dependence of these parameters (Gibbons et al., 1961).

The exact integrations of the Mie functions can now be used to check a previous approximation by Deirmendjian (1957, 1959) based on the W.K.B. method. In that paper, the Mie phase functions were underestimated by a factor 4π (1959, equations (15), (16) and Table 3) because of an oversight in the definition of the amplitudes of the scattered field. Taking this into account, the following table gives a comparison of the approximate and exact calculations for a model C haze at $\lambda 0.45\mu$:

	Phase function $P_1(\theta)$, model C haze				
θ	$0^\circ.25$	1°	3°	6°	10°
W.K.B. method (Deirmendjian, 1959)	562	157	59.3	31.5	18.3
Exact Mie functions (this paper)	74.7	67.1	38.1	20.0	14.7

The large deviations appearing above are explained by the incorrect integration with respect to a model C distribution rather than by the W.K.B. approximation itself, which is very good for individual particles at small scattering angles (Deirmendjian, 1957). In fact, if the original integration of the diffracted intensity were carried to a realistic finite upper limit of the particle size, instead of an

infinite limit as in the Struve integral (Deirmendjian, 1959, p. 231), the use of the W.K.B. approximation should result in very good estimates of the aureole for this particular model. Furthermore, if a distribution of the type (1) is used instead, the convergence property mentioned in the second section of this paper, suggests that in the diffraction area, definite integrals of the form

$$\frac{1}{\sin^2\theta} \int_0^\infty x^{2+\alpha} e^{-bx} \left[J_1(x\sin\theta)\right]^2 dx$$

must exist, with a finite value even for $\theta = 0$.

Figures 6 to 9 present the normalized intensity obtained from a cloud-drop size distribution described by (5). Figure 6 corresponds to infrared illumination at $\lambda 10\mu$. A considerable anisotropy and strong maximum polarization at $\theta \approx 110^\circ$ are evident, even for this long wavelength; otherwise the angular scattering pattern is quite smooth. The next case, shown in Fig. 7, can be compared with Fig. 2 for haze. It is seen that in the cloud model a maximum positive polarization occurs at $\theta = 152^\circ$, in a broad, secondary maximum in the intensity, corresponding to an infrared rainbow. The anisotropy is high with a ratio of about 10^3 between forward and back scatter.

Going towards the visible, Figs. 8 and 9 show the very interesting patterns for a cloud illuminated by $\lambda 0.70$ and $\lambda 0.45\mu$ radiation, respectively. Note first the very pronounced aureole or diffraction peak in the region $0^\circ \leqq \theta < 5^\circ$, which is twice as bright in the blue as in the red near 0°. This undoubtedly accounts for the very bright "silver lining" at the borders of certain clouds when near the sun. Next, in the region $20^\circ < \theta < 80^\circ$, the intensities fall

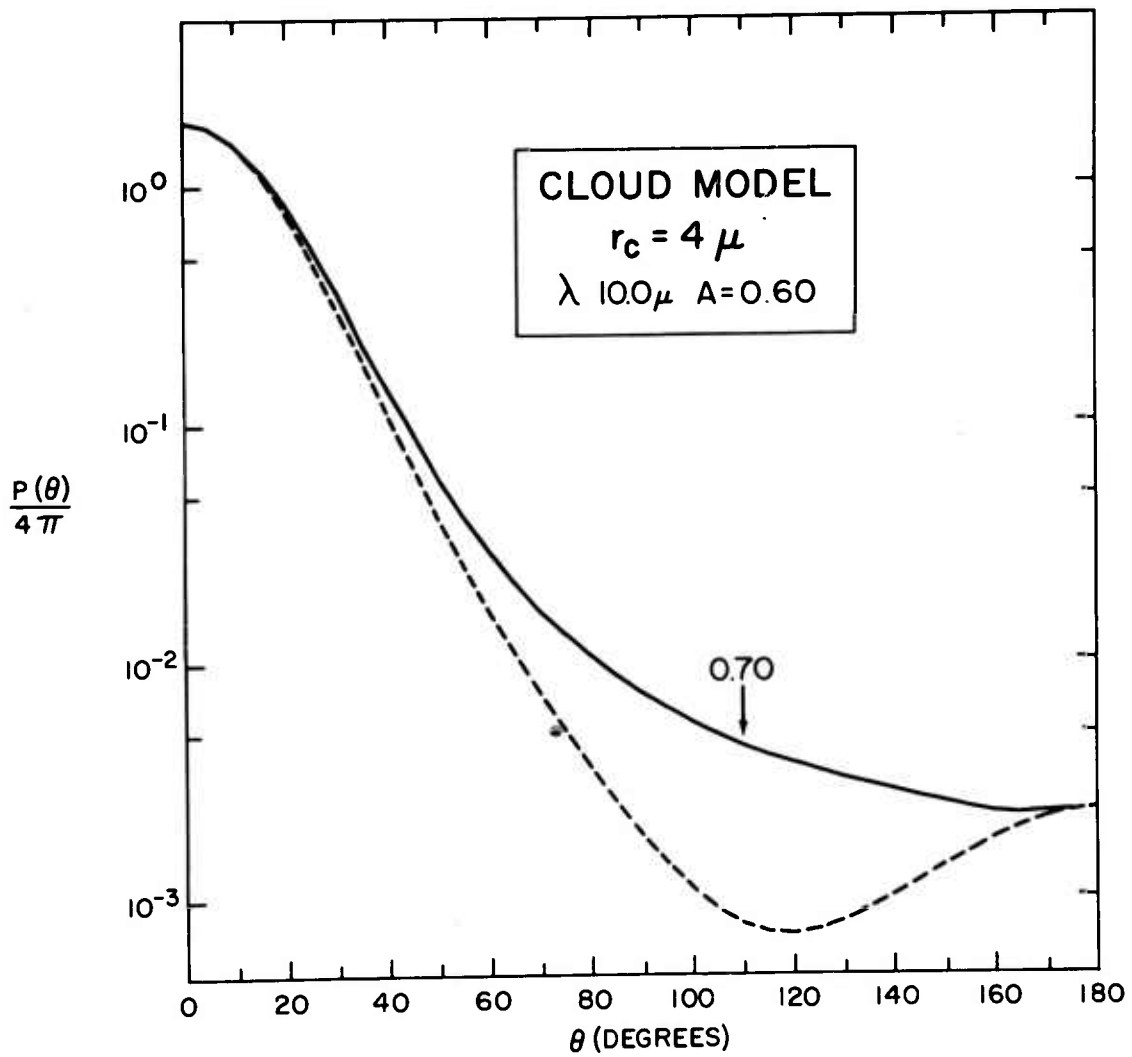

Fig. 6

Intensity functions for a water cloud illuminated by $\lambda 10\mu$ infrared radiation. Computed values at θ: $0(5)180^\circ$.

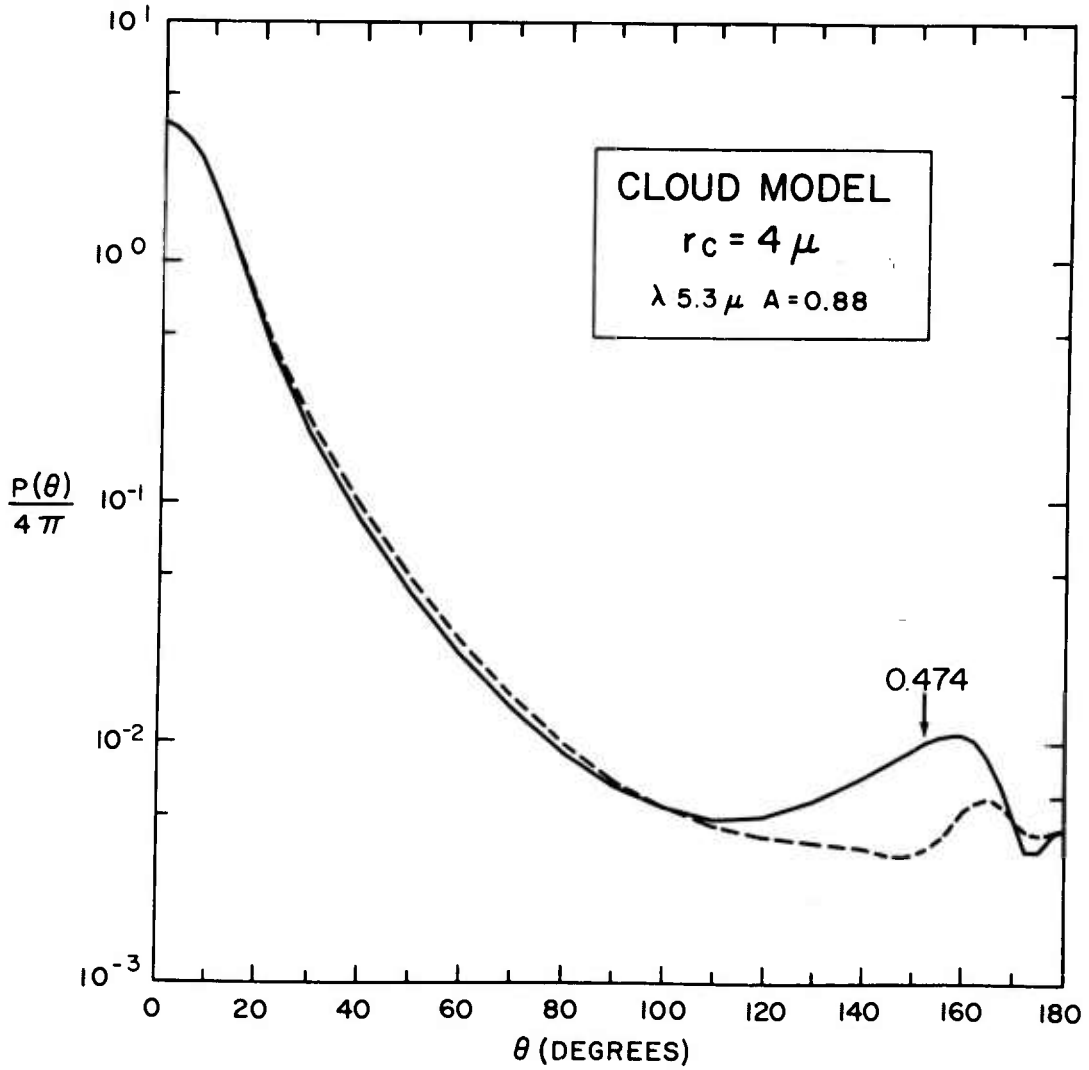

Fig. 7

Same as Fig. 6 but at $\lambda 5.3\mu$.

Computed values at θ: 0(2.5)30(10)140(2.5)180°.

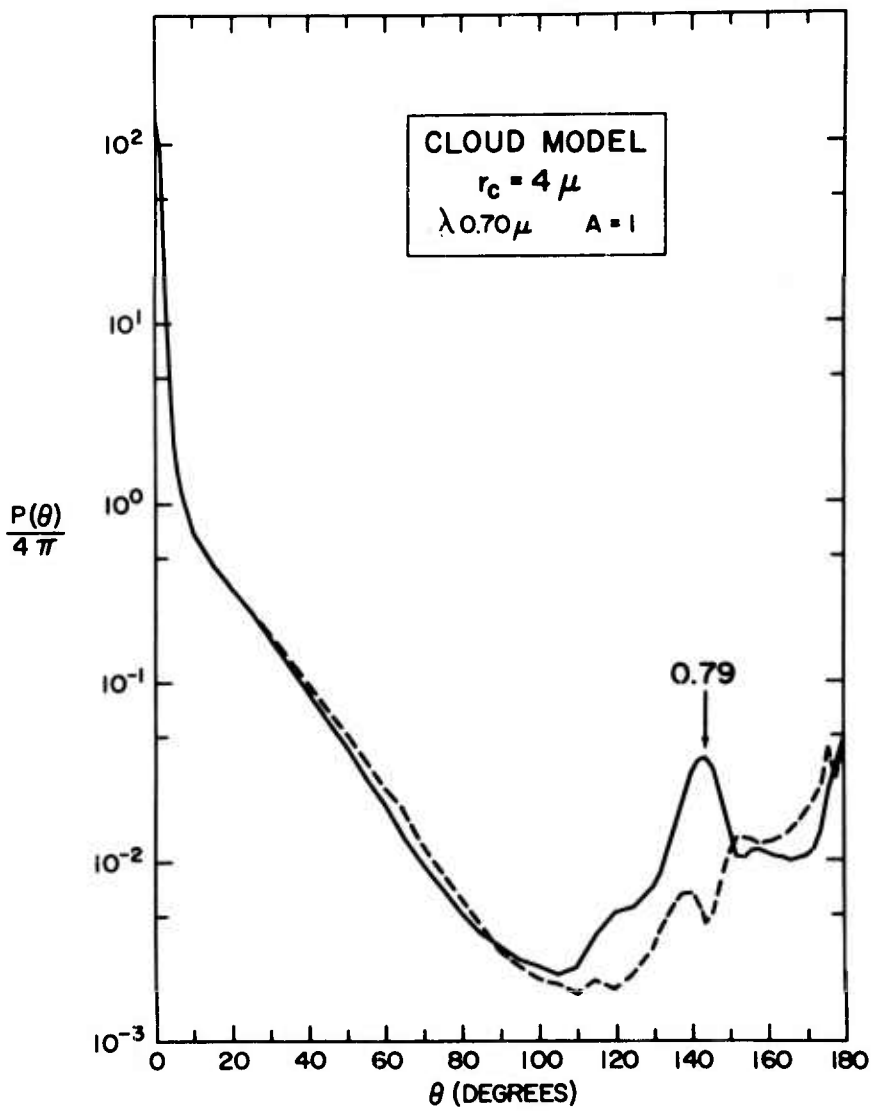

Fig. 8

Same as Fig. 6 but at $\lambda 0.70\mu$ and real index 1.33.
Computed values at θ: 0(1)10(5)130(2)180°.

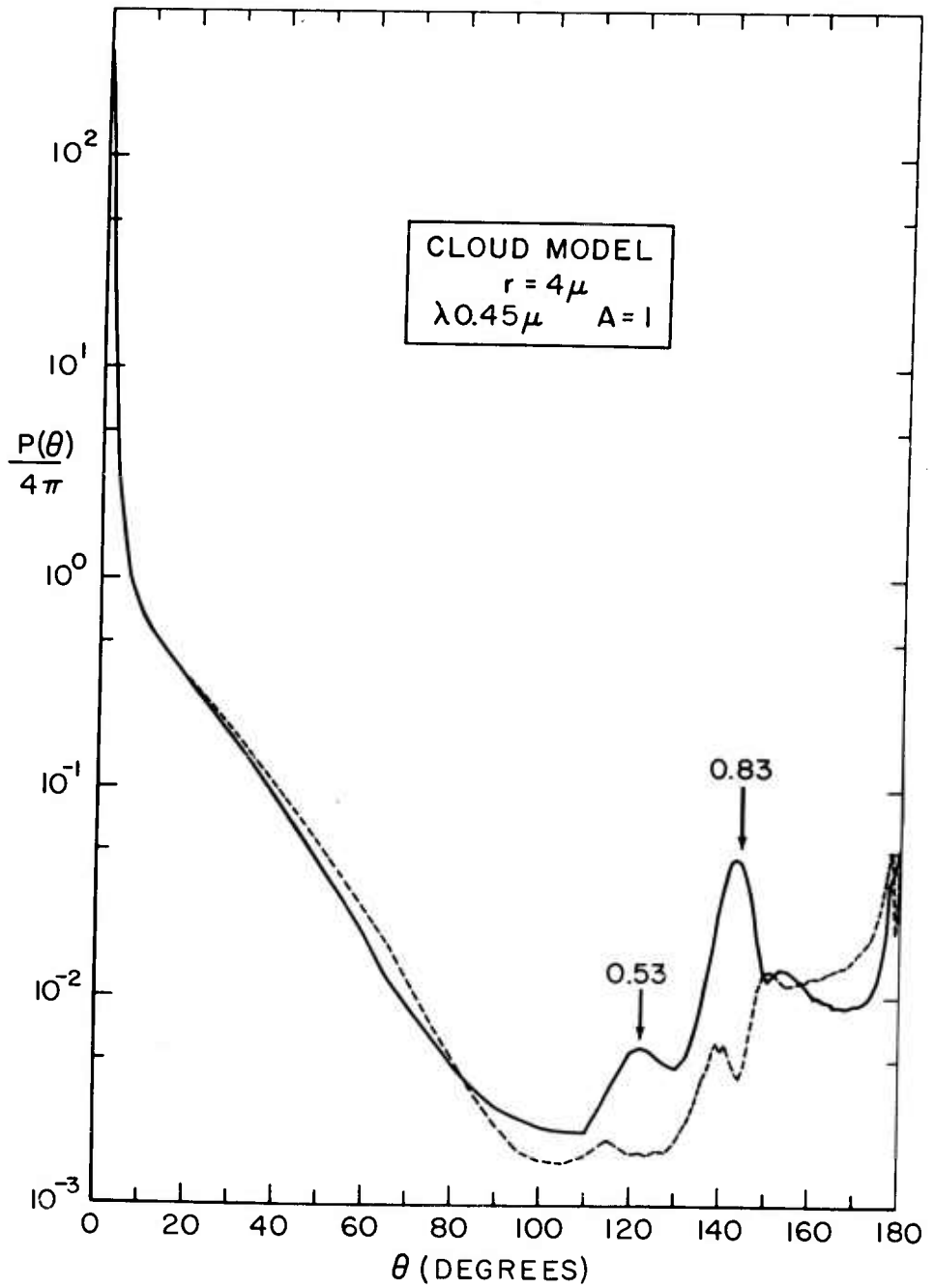

Fig.9 — Same as Fig.6 but at λ0.45μ and real index 1.34
Computed values at θ: 0(1) 15(5) 120(2) 132(1) 180°

exponentially with the scattering angle, with little or no polarization change. The region $80^\circ < \theta < 110^\circ$ corresponds to a minimum in intensity and change in the sign of the polarization.

The region $110^\circ < \theta \leqq 180^\circ$ contains distinct features which deserve discussion. The most salient of these is of course the pronounced and relatively narrow maximum around $\theta = 143^\circ$. This is the fogbow or white rainbow mentioned by Minnaert (1954, p. 183). Comparing Figs. 8 and 9, we see that there is no true dispersion, the blue bow maximum corresponding to the red in position. However, the blue bow is narrower and more intense and its polarization exceeds that of the red bow. This must be explained in terms of the larger relative size of the cloud drops with respect to the wavelength. This trend indicates that the polarization in the true rainbow should be even greater. Furthermore, in the true rainbow, which occurs at about $\theta = 138^\circ$, the condition $x \longrightarrow \infty$ applies to all wavelengths and the dispersion must be mostly due to the refrangibility of water. The interesting fact that emerges from the present study is that a wide size distribution in cloud droplets does give rise to a single principal bow so that all the secondaries and supernumeraries, which appear by scattering on single cloud droplets, are virtually suppressed by superposition. There is an indication of a weak secondary bow around $\theta = 122^\circ$ at $\lambda 0.45\mu$ only.

Similarly the appearance of a counter corona of radius of about 2° at $\lambda 0.45\mu$ and 4° at $\lambda 0.70\mu$ is interesting for the same reason. The author has actually observed this visually on the vertical wall of a towering cumulus from a jet airliner at about 30,000 feet, with

the sun near the horizon. Note that the polarization in the counter-corona has the opposite sign from that of the rainbow. No direct coronas were found in this model, however, because of the wide size distribution assumed.

Comparisons with observations and other work

A most remarkable corroboration of the above cloud model comes from the careful angular scattering and polarization measurements made at night by Pritchard and Elliott (1960) with their recording polar nephelometer on small volumes of natural fog (their Fig. 13). These measurements, made with a green filter, reproduce quite faithfully most of the salient features appearing in Figs. 8 and 9, including the intense aureole, the exponential decrease and other gradients, position of the minimum, position and intensity of the rainbow and its polarization (the components VV and HH of Pritchard and Elliott, 1960, are proportional to the elements P_1 and P_2 respectively). Apparently it was not possible to cover the range $170^\circ < \theta \leqq 180^\circ$, hence the counter corona and backward peak are not present. Considering that the observations correspond to ground fog, in which the size distribution is not necessarily that of a cumulous cloud as in our model, the agreement is indeed remarkable. Also the measurements include the effects of molecular scattering which must have some influence on the polarization around $\theta = 100^\circ$ (see Equation (13)).

The measurements on clear nights by Pritchard and Elliott (1960) also show good agreement with our haze models except in the polarization, whose maximum does appear at $\theta = 100^\circ$ but has a larger

value than shown on Figures 3 or 5, for example, because of the strong influence of molecular scattering at this angle.

The theoretical curves should also be compared with measurements of the angular intensity only, in the range $16^\circ \leqq \theta \leqq 164^\circ$ reported by Barteneva (1960), whose work, however, is not as detailed as that of Pritchard and Elliott.

Integrations somewhat similar to ours, but not normalized with respect to the integrated scattering cross-sections, and carried out to the constant upper limit of $x_2 = 40$, with an interval of $\Delta x = 1$, have been reported by Giese (1961). In contrast, for example, our integration intervals and range in x for Figure 9 is 0.25(0.25)60(0.50)160. Furthermore Giese has used distribution functions of the type $n(r) \sim r^{-\alpha}$ with $\alpha = 2, 2.5, 3$ appropriate to zodiacal particles. It is interesting to note that samples of his results (Giese, 1961, Fig. 9a) show some of the features appearing in our cloud model, including a broad rainbow around $\theta = 140^\circ$, even though his size range corresponds to a haze model. This is explained by the size distribution function used by Giese, which is considerably less steep than in our models C and M.

One very interesting observational peculiarity of scattering on polydisperse Mie particles must be mentioned, whose theoretical corroboration could be provided only by computing the <u>normalized</u> intensities as in the present case. This is the apparent constancy of the quantity $(P_1+P_2)/8\pi$ around $\theta = 40^\circ$, with a value of about 0.1 regardless of the size distribution function, as evidenced by Figs. 4, 5, 8 and 9. A check into our tabulated values shows that

this is true even if the integration is stopped at smaller sizes, provided these exceed the first resonance peak in the scattering cross-section. This behavior suggests that for small samples of a polydisperse suspension, the concentration of the particles is directly proportional to the measured intensity scattered around $\theta = 40^{\circ}$, regardless of the size distribution and maximum size of the particles, provided the distribution is continuous and of the type (1), and the index of refraction is real and remains unchanged. The experimental facts are provided by the analyses of two independent sets of observations made on entirely different media, to wit, those reported by Barteneva and Bashilov (1961) for atmospheric aerosols, and those of Tyler (1961) for hydrosols. Both papers reveal a very good linear correlation between the scattering function at $\theta = 45^{\circ}$ and the volume scattering coefficient or degree of turbidity. This property is also mentioned in a very interesting review paper by G. V. Rosenberg (1960).

The functions P_3 and P_4

The functions P_3 and P_4 integrated and normalized according to (9) have to do with a rotation of the plane of polarization and introduction of elliptical polarization by polydisperse suspensions, when illuminated by polarized light. These will not be discussed in detail here, except to show one example in Fig. 10 corresponding to Model M at $\lambda 0.70\mu$. The functions $P_3(\theta)/4\pi$ (solid line) and $P_4(\theta)/4\pi$ (dashed line) are plotted linearly against the scattering angle. For comparison, the corresponding Rayleigh value for $P_3(\theta)/4\pi$ is shown by the dotted line (the Rayleigh value for P_4 is zero

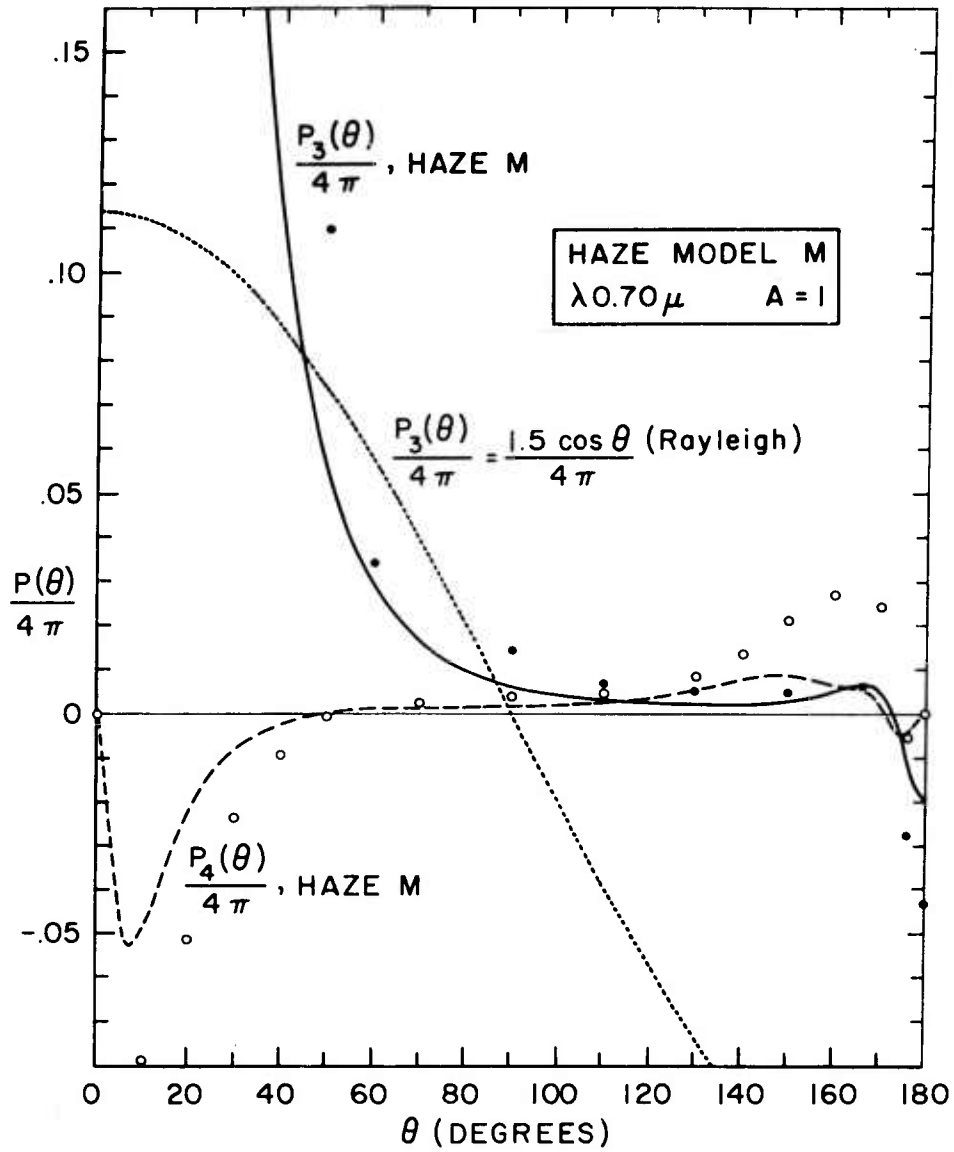

Fig.10— Integrated and normalized functions $P_3/4\pi$ (solid line) and $P_4/4\pi$ (dashed line) for haze particles at $\lambda 0.70\mu$. Comparable values, shown by solid and open dots, respectively, for a different size distribution and refractive index, adapted from Fraser (1959, p.123, "model D")

everywhere). There are no experimental values that could be used for comparison here. Comparable values computed by Fraser (1959) are shown by solid and open dots in Fig. 10. Although the latter were computed for m = 1.40 and a different size distribution and range, there is general agreement in the order of magnitude, the gradient and the position of the maxima. Fraser's results are based on a Legendre series expansion due to Sekera (1957), using the Mie scattering coefficients a_n and b_n, which are independent of θ. The general agreement mentioned above is proof of the correctness of the method. However, the possibility of accurately generating the complex scattered amplitudes by means of high-speed computers (Deirmendjian et al, 1961), allows a much more reliable direct integration of these parameters.

Some conclusions

On the basis of this limited sample of our results and comparison with available observations, the following conclusions may be reached:

a. The classical electromagnetic theory of scattering on homogeneous finite spherical particles, applied to a polydispersed suspension with a continuous size distribution, can be used to reproduce rather accurately the observed angular intensity and linear polarization of samples of natural water clouds and hazes illuminated by visible light.

b. No single particle in such a suspension exists, whose angular scattering and polarization properties correspond to the integrated effects from all the particles, which tend to suppress by

superposition the extreme angular fluctuations characteristic of single particles. The introduction of such parameters as the "mean radius," the "mode radius," the "mean volume radius," etc., is not helpful in determining these properties for aggregates of particles, except perhaps in the case of very small particles relative to the wavelength. Our results further indicate that the angular volume scattering properties are uniquely determined by the type of size distribution, the range of sizes, and the dielectric and conducting properties of the particles in the suspension, independently of the total concentration. Hence, in the case of optically thin samples of such suspensions (where multiple scattering is negligible), these parameters may be deduced from careful measurements of the scattering properties in as many directions as possible and at various wavelengths.

c. The existence of a solution to the analogous general problem in the case of optically thick media, i.e., that of the unique determination of the type, size, size distribution, and size range of the particles in suspension, from a knowledge of the angular intensity and polarization of the diffusely transmitted and reflected radiation, as discussed by other participants in this symposium, remains to be demonstrated. However, in the case of certain suspensions such as water-droplet clouds in the atmosphere, the existence of prominent features such as rainbows and counter coronas suggests that some information on the size and size distribution of the particles may be obtained from these features, which should be observable on diffuse reflection even against the background of the multiply

scattered field.

d. The calculation of the normalized scattered intensities corroborates the experimental result that, at least in the case of dielectric particles, the intensity at a fixed scattering angle around 45° is directly proportional to the total number concentration per unit volume independently of the size distribution and size range. Thus under certain conditions and for optically thin media, the concentration or degree of turbidity may be obtained by this method as well as by the usual one based on the extinction of a collimated beam.

ACKNOWLEDGMENT

R. J. Clasen programmed the generation and integration with respect to size of the Mie functions on the IBM 7090 computer.

List of References

Barteneva, O. D. (1960) Bull. Acad. Sci. U.S.S.R., Geophys. Ser. No. 12, 1237 (in A.G.U. translation).

Barteneva, O. D. and G. Ya. Bashilov (1961) Bull. Acad. Sci. U.S.S.R., Geophys. Ser. No. 4, 395 (in A.G.U. translation).

Centeno, M. (1941) J. Opt. Soc. Amer. 31, 244.

Chandrasekhar, S. (1950) Radiative Transfer, Clarendon, Oxford.

Deirmendjian, D. (1957) Ann. Geophys. 13, 286.

Deirmendjian, D. (1959) Ann. Geophys. 15, 218.

Deirmendjian, D. (1960) Quart. J. R. Met. Soc. 85, 404.

Deirmendjian, D., R. Clasen and W. Viezee (1961) J. Opt. Soc. Amer. 51, 620.

Durbin, W. G. (1959) Tellus 11, 202.

Fraser, R. S. (1959) Dissertation, U. Calif., Los Angeles. (see also Sci. Rep. No. 2, Contract No. AF 19(604)-2429, AFCRC-TN-60-256, 1959).

Gibbons, M. G., J. R. Nichols, F. I. Laughridge and R. L. Rudkin (1961) J. Opt. Soc. Amer. 51, 633.

Giese, R. H. (1961) Zeits. Astrophys. 51, 119.

Gilbert, J. Y. (1954) Condensation Nuclei of the Los Angeles Region, U. of Calif., Dept. Meteor., Los Angeles.

van de Hulst, H. C. (1957) Light Scattering by Small Particles, Wiley, New York.

Junge, C., C. W. Chagnon and J. E. Manson (1961) J. Meteor. 18, 81.

Khrgian, A. Kh and I. P. Mazin (1952) Trudy Tsentral. Aerolog. Observat. No. 7, 56

Khrgian, A. Kh and I. P. Mazin (1956) Trudy Tsentral. Aerolog. Observat. No. 17, 36.

Minnaert, M. (1954) The Nature of Light and Colour in the Open Air, Dover, New York.

Penndorf, R. (1962) J. Opt. Soc. Amer. 52, 402.

Pritchard, B. S. and W. G. Elliott (1960) J. Opt. Soc. Amer. 50, 191.

Rosenberg, G. V. (1960) Soviet Physics Uspekhi, 3, 346 (in Amer. Inst. Phys. transl.)

Sekera, Z. (1957) Hand. Phys. 48, 288.

Singleton, F. and D. J. Smith (1960) Quart. J. R. Met. Soc. 86, 454.

Tyler, J. E. (1961) J. Opt. Soc. Amer. 51, 1289.